New VHP-Female v. 2.0 Full-Body Computational Phantom and Its Performance Metrics Using FEM Simulator ANSYS HFSS

Janakinadh Yanamadala, *Member, IEEE*, Gregory M. Noetscher, *Member, IEEE*, Vishal K. Rathi, *Member, IEEE*, Saili Maliye, Htay A. Win, *Member, IEEE*, Anh L. Tran, Xavier J. Jackson, Aung T. Htet, Mikhail Kozlov, *Senior Member, IEEE*, Ara Nazarian, Sara Louie, *Senior Member, IEEE*, and Sergey N. Makarov, *Senior Member, IEEE*

***Abstract*— Simulation of the electromagnetic response of the human body relies heavily upon efficient computational models or phantoms. The first objective of this paper is to present a new platform-independent full-body electromagnetic computational model (computational phantom), the Visible Human Project® (VHP)-Female v. 2.0 and to describe its distinct features. The second objective is to report phantom simulation performance metrics using the commercial FEM electromagnetic solver ANSYS HFSS.**

I. Introduction

Numerical simulation of the electromagnetic and thermal response of the human body to different stimuli in MRI safety, electromagnetic tomography, and electromagnetic stimulation is currently limited by the availability of anatomically adequate and numerically efficient cross-platform computational models [1-5]. Platform-independent and efficient models suitable for all three major electromagnetic simulation methods, i.e. Finite Element Method (FEM), Method of Moments or Boundary Element Method, and Finite-Differences Time Domain, which are based on triangular surface meshes of individual tissues, become increasingly important today. The first objective of this paper is to present a new platform-independent full-body electromagnetic computational model (computational phantom), the Visible Human Project® (VHP)-Female v. 2.0, and to describe its distinct features. The second objective is to report phantom simulation performance metrics using the commercial FEM electromagnetic solver ANSYS HFSS for two tasks: plane wave incidence and MRI-coil modeling.

II. Phantom Description

A. Number of Parts, Image Source, and Accuracy

The computational phantom VHP-Female v. 2.0 includes 190 individual tissue parts to date in the form of finite-element triangular surface meshes with approximately 150,000 triangles total. Each tissue part has been extracted from the Visible Human Project®-Female dataset [6] of the National Library of Medicine using the available cryosection images with a pixel resolution of 0.33 mm, which provide state-of-the-art resolution of muscle and other soft tissues, as well as bone matter. The surface deviation error between the true surface and its triangulation in the normal direction does not exceed 0.5-2 mm in the cranium and 6 mm in the main body.

B. Topology of Triangular Surface Meshes

The phantom possesses a set of topological characteristics necessary for cross-platform compatibility and computational efficiency. Each original tissue triangular surface mesh is strictly 2-manifold or thin-shell (no non-manifold faces, no non-manifold vertices, no holes, and no self-intersections). No tissue mesh has any triangular facets in contact with other tissue surfaces. There is always a (small) gap between the distinct tissue surfaces. This gap physically represents thin membranes separating distinct tissues. Numerically, it corresponds to an "average body" container(s), which encloses organs and tissues, and guarantees compatibility between different CAD formats. At the same time, there exist tissues fully enclosed within each other, such as the white matter inside the gray matter, cancellous bone inside a cortical bone shell of the femur, etc. These tissues also neither touch nor intersect. Each tissue triangular surface mesh has the minimum surface triangular mesh size allowed. The entire phantom and the individual tissue surface meshes are available in MATLAB binary format as well as in a variety of standard CAD formats. Fig. 1 shows the phantom meshes within the MATLAB shell.

III. Phantom Features

A. Improved Resolution in the Cranium

The VHP-Female head shown in Fig. 2a is less detailed than the world standard model [7]. And yet, one unique feature of its head is an anatomically-correct continuous shell of the highly-conductive cerebrospinal fluid (CSF) with a variable thickness of 1-7 mm, which maintains a shorting path of electric current. Further, the CSF shell has a direct connection with the spinal cord. The shell continuity is critical for accurate direct-current modeling such as EEG, electric impedance tomography, and direct-current stimulation [8]-[11]. Therefore, the cranium model has already been used for research purposes [12],[13]. Additionally, there are two 0.3mm thick shells around the CSF shell shown in

J. Yanamadala, G.M. Noetscher, V. K. Rathi, S. Maliye, H. A. Win, A. L. Tran, A.T. Htet and S.N. Makarov are with the Electrical and Computer Eng. Dept. at Worcester Polytechnic Institute, Worcester, MA 01604 USA (phone: 508-831-5017; e-mail: makarov@wpi.edu).

X. Jackson is with the Bioinformatics and Computational Biology Dept. at Worcester Polytechnic Institute, Worcester, MA 01604 USA (e-mail: xjjackson@wpi.edu).

M. Kozlov is with the Department of Neurophysics at the Max Plank Inst. for Human Cognitive and Brain Sciences in Leipzig, Germany (e-mail: kozlov@cbs.mpg.de).

S. Louie is with ANSYS, Inc., Canonsburg, PA (email: sara.louie@ansys.com).

A. Nazarian is with the Center for Advanced Orthopaedic Studies at Beth Israel Deaconess Medical Center, Harvard Med. School, Boston, MA (e-mail: anazaria@bidmc.harvard.edu)

978-1-4244-9270-1/15/$31.00 ©2015 IEEE

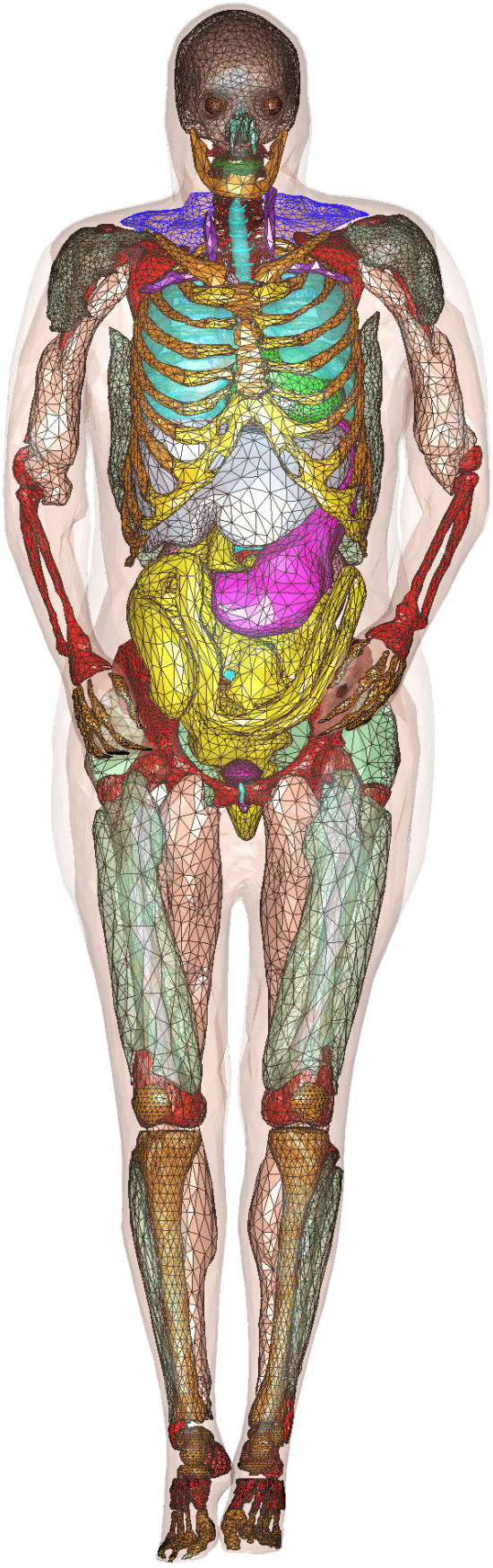

Figure 1. Anterior view of the VHP-Female computational phantom v. 2.0 within the MATLAB shell. Skin layer and some muscles are not shown.

Fig. 2b,c, respectively. These shells may either model brain membranes or CSF expansions.

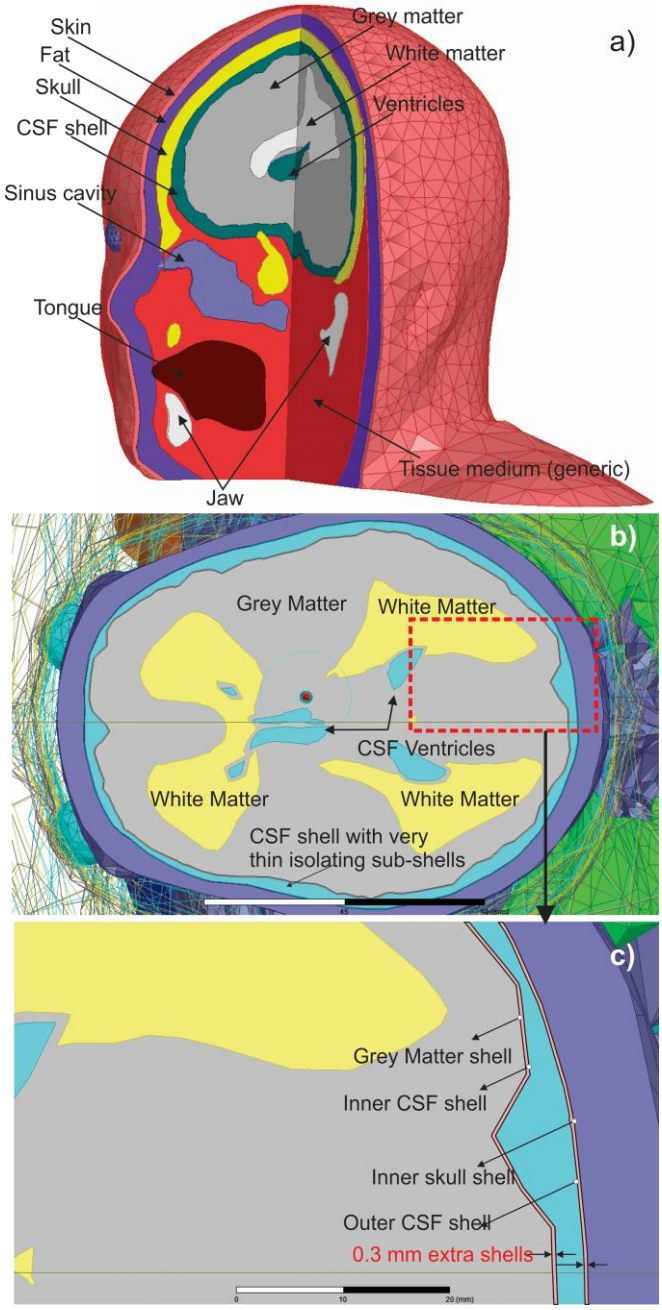

Figure 2. Cranium of the VHP-Female v. 2.0 phantom. CSF shell and additional thin layers are shown.

B. Variable BMI

Estimation of the Body Mass Index (BMI) using the original phantom outer fat shell predicts a value of approximately 36, classifying the patient as obese. This fat shell and the average body container have been simultaneously deformed in order to model medium and low BMI values. The corresponding result is shown in Fig. 3. All other tissue meshes remain the same. This method is indeed somewhat inaccurate anatomically, but may perhaps be used for integral MRI estimates and assessing fat layer impact on Specific Absorption Rate (SAR).

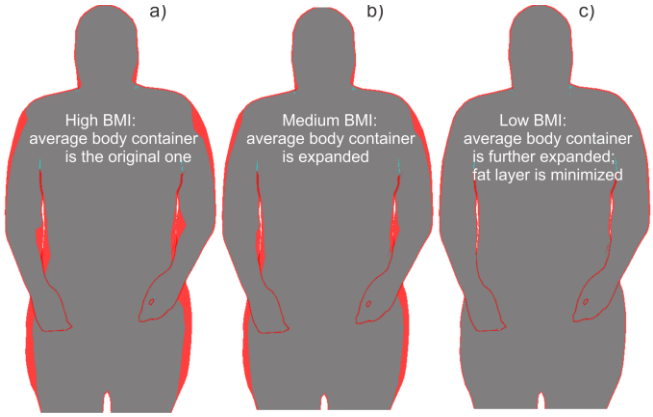

Figure 3. Three different fat shells used with the VHP-Female v. 2.0 phantom.

C. *Bone Composition and Addition of Large Orthopedic Implants*

Special attention motivated by ongoing osteoporotic studies has been paid to the vertebral column [14] and to large femoral bones shown in Fig. 4a. In the latter case, surface extraction has been accurately performed for three distinct bone tissues: cortical, trabecular, and bone marrow. Based on current practices, the femoral and neighboring meshes have been deformed in order to register and embed three large orthopedic metallic implants shown in Figs. 4b-d. The implants originate from the Center for Advanced Orthopaedic Studies, Beth Israel Deaconess Med. Center (BIDMC), Harvard Med. School. All other tissue meshes remain the same. Large implants may cause extra MRI heating; this effect is an active area of research today [15].

D. *Conversion from Triangular Surfaces to NURBS Surfaces (B-Splines)*

NURBS surfaces enable (adaptively) refined meshes without sharp edges (where charge density becomes singular) in specific areas of interest. Furthermore, they can be used for deformation purposes [16]. Otherwise, the NURBS surfaces have a limited value for an FEM solver, which internally operates with geometry primitives: triangular facets and tetrahedra. A double conversion, from segmented triangular surfaces→NURBS surfaces→FEM triangular surfaces, may require a (very) significant additional meshing time. Fig. 5 shows a conversion from the original triangulated surface of the VHP-Female skin shell (about 7,000 triangles) to a set of NURBS surfaces (about 60 B-splines) done with SpaceClaim Direct Modeler of ANSYS. Eventually, we plan on converting the entire VHP-Female model to NURBS surfaces.

E. *Phantom Validation*

Selected parts of the phantom were evaluated by medical professionals from BIDMC. MRI field simulation results, (some of which are reported below) for a 1.5 T coil have shown an agreement with experimental measurements of B_1+. Those results will be reported separately.

IV. Computational Performance Using High-Frequency FEM Simulator ANSYS HFSS

A. *Plane Wave Test*

An ANSYS HFSS project has been created for a plane wave incident upon the phantom at 300 MHz using 5 passes of

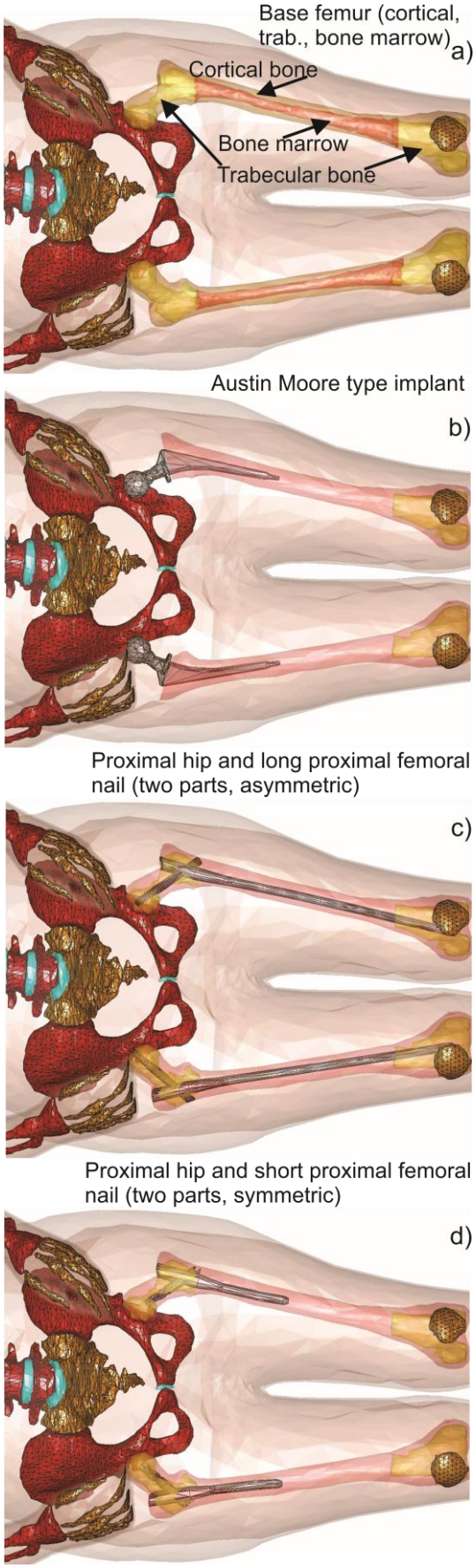

Figure 4. Bone composition and femoral implants registered with the VHP-Female phantom. Soft tissues are not shown.

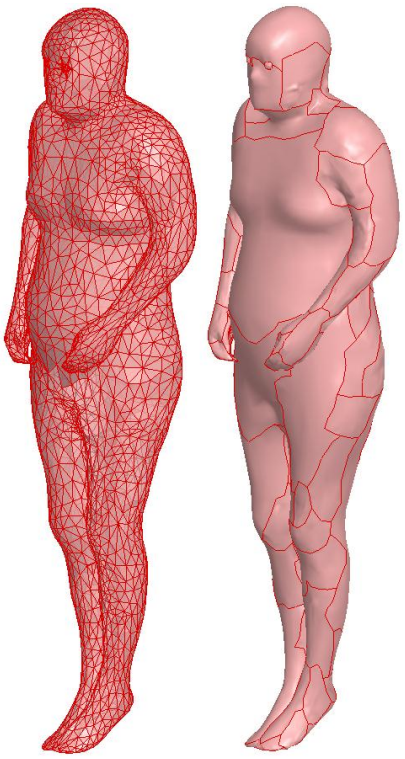

Figure 5. Left- initial triangular surface of the VHP-Female; right – the same surface converted to B-splines.

adaptive mesh refinement and integral-equation boundary conditions for a box which tightly surrounds the body. The adaptive solution process is the method by which HFSS guarantees that the final FEM solution is the correct one. Table I reports simulation benchmarks for four representative computational servers. Final delta Magnitude Energy (or delta E) is *less than 0.015*. For a single adaptive pass, a global normalized error function in the frequency domain is the ratio of the reaction integral magnitude to the total system energy in the computational volume V (Ref. [17], Eq. (43))

$$\delta = \frac{\int \left| \vec{E} \cdot \vec{J} - \vec{H} \cdot \vec{M} \right| dV}{\omega \times \frac{1}{2} \int \left| \varepsilon \vec{E} \cdot \vec{E} + \mu \vec{H} \cdot \vec{H} \right| dV} \qquad (1)$$

where $\vec{E}$, $\vec{H}$ are electric and magnetic fields, and $\vec{J}$, $\vec{M}$ are electric and magnetic current densities. The reaction integral is exactly zero in a source-free field and is a constant when the sources are somewhere present. The delta E is the difference in two values of δ from Eq. (1), for two consecutive passes. As the solution converges to the exact result, delta E, which is the global convergence criterion, approaches zero for any source distribution.

Two conclusions can be made based on these and similar results: (i) Intel processors are more beneficial for use with ANSYS HFSS and (ii) the use of distributed or high-performance computing decreases the elapsed time for accurate full-body FEM simulations related to radar cross-section/antenna modeling to about 4 hours total. However, the dependence on the number of cores is nonlinear; eight cores and one task are recommended, with the RAM limit of 130—160 GB. Note that the classic mesher, not the τ-mesher, was enforced in HFSS (HFSS→ Mesh operations →Initial mesh settings →Meshing Method). The τ-mesher causes prohibitively large execution times and should perhaps be not used for this application.

TABLE I. SIMULATON BENCHAMARKS FOR PLANE WAVE TEST – ANSYS ELECTROMAGNETIC SUITE RELEASE 15/16

Execution results for four representative servers		
System	***Tetrahedral mesh size & total RAM (start/stop)***	***Execution time for 5 passes***
System #1 (one task, one core)		
Intel(R) Xeon(R) CPU E5-2697 V2, 256 GB, 64-bit OS Windows Server 2008 R2 Enterprise ANSYS EM Suite® 16.0.0	450,000/1,000,000 2.6GB/87 GB	Meshing time: 50 min Sim. time: 10 hr 48 min
System #2 (one task, one core)		
4 AMD OPTERON 6174 12 core processors, 192 GB, 64-bit OS, Windows Server 2008 R2 Enterprise ANSYS EM Suite® 15.0.2	450,000/1,000,000 2.0GB/115 GB	Meshing time: 70 min Sim. time: 28 hr 55 min
System #3 (one task, one core)		
Intel(R) Xeon(R) CPU E5-2690, 192 GB, 64-bit OS Red Hat Enterprise Linux 2.6.32 ANSYS EM Suite® 15.0.2	450,000/1,000,000 2.0 GB/87 GB	Meshing time: 63 min Sim. time: 10 hr 40 min
System #4 (one task, eight cores, HPC option)[a]		
Intel(R) Xeon(R) CPU E5-2697 V2, 256 GB, 64-bit OS Windows Server 2008 R2 Enterprise ANSYS EM Suite® 16.0.0	450,000/1,000,000 2.6GB/87 GB	Meshing time: 50 min Sim. time: 2 hr 43 min

a. Systems 1 and 4 differ by the HPC option only.

TABLE II. SIMULATON BENCHAMARKS FOR FULL-BODY MRI COILS – ANSYS ELECTROMAGNETIC SUITE RELEASE 15.0.2, INTEL(R) XEON(R) 3 GHZ DELL WORKSTATION.

Execution results for different coil/mesh configurations (6 cores, HPC option, manual coil meshing). Final relative delta S is less than 0.002		
Configuration	***Tetrahedral mesh size & total RAM (start/stop)***	***Execution time for 2 passes***
1.5 T coil, 64 MHz, 48 excitations, head only	3,200,000/4,000,000 3.4GB/91.6 GB	Meshing time: 3 h 15 min Sim. time: 6 hr 8 min
3 T, 128 MHz, 48 excitations, head only, interpolating sweep	2,600,000/3,300,000 3.2GB/62.7 GB	Meshing time: 2 h 6 min Sim. time: 7 hr 42 min
3 T, 128 MHz, 48 excitations, whole body	4,000,000/5,000,000 4.5GB/134 GB	Meshing time: 4 h 30 min Sim. time: 4 hr 39 min
3 T, 128 MHz, 48 excitations, whole body	5,400,000/6,400,000 5.9GB/121 GB	Meshing time: 5 h 20 min Sim. time: 14 hr 22 min

B. MRI-Coil Modeling

One MRI coil utilized was a 64 MHz high pass 16 rung birdcage design with dimensions relevant to clinical 1.5 T scanners: coils of diameter 604 mm and length 650 mm as

described in Ref. [15]. Yet another similar coil operated at 128 MHz and 3 T. The coil is using 48 excitation ports because this setup allows one to obtain near-field results for any kind of coil tuning (high pass, low pass, band pass) without re-running 3D EM simulations. Table II reports selected simulation benchmarks for head and full-body scans, with two adaptive meshing passes. Manual meshing in critical areas has been used prior to the adaptive mesh refinement. The convergence criterion is now delta S, which is the magnitude of the change of the terminal S-parameters (the largest magnitude is selected) between two consecutive passes. This manual meshing guarantees that the final relative delta S is *less than 0.002*, even with only two adaptive passes. This value underscores the importance of manual meshing for modeling the human phantom augmented with external electromagnetic hardware.

V. Conclusion and Future Work

In this study, we have presented the VHP-Female v. 2.0 computational phantom and described its initial performance metrics using the FEM high-frequency electromagnetic simulator ANSYS HFSS. Similar estimates have been obtained for the low-frequency EM simulator Maxwell 3D of ANSYS. For a plane wave test (and similar antenna/array tasks), the one-core run time is about twelve hours on average while the multi-core run time is less than four hours, yielding a final relative energy error of less than 0.015 (after five adaptive passes). For the most complicated MRI-related simulations with manual meshing, the total multicore run time is about nine to twenty hours, while maintaining a very good solution accuracy. Thus, the VHP-Female v. 2.0 full-body phantom will provide a reasonably fast yet accurate and flexible computational platform for multi-purpose electromagnetic modeling of a multi-tissue human body. We believe the phantom is suitable for thermal and acoustic modeling as well. The Worcester Polytechnic Inst. Institutional Review Board (IRB) has reviewed the materials submitted in regards to the above mentioned study and has determined that this research is exempt from further IRB review and supervision under 45 CFR 46.101(b) (HHS IRB # 00007374).

Ongoing work is directed toward improving anatomical accuracy, mesh quality, and flexibility of the phantom while maintaining approximately the same or even shorter simulation run times.

Acknowledgment

Authors are thankful to Dr. Alexander Prokop of Computer Simulation Technology, AG for testing the model with CST Microwave Studio and useful discussions. This material is based upon work supported by the National Science Foundation under Grant No. 1520168, Platform-Independent Full-Body Computational Human Phantom.

References

[1] IEEE International Committee on Electromagnetic Safety: Technical Committee 34: List of available human phantoms: http://grouper.ieee.org/groups/scc34/sc2/wg2/available%20human%20models.doc

[2] K. Genc, P. Segars, S. Cockram, D. Thompson, M. Horner, R. Cotton, and P. Young, "Workflow for creating a simulation ready virtual population for finite element modeling," in *2013 Proc. ASME/FDA* 1st Annual Frontiers in Medical Devices: Applications of Computer Modeling and Simulation, FMD2013, Sep. 11-13, 2013, Washington, DC.

[3] A. Christ, W. Kainz, E. G. Hahn, K. Honegger, M. Zefferer, E. Neufeld, W. Rascher, R. Janka, W. Bautz, J. Chen, B. Kiefer, P. Schmitt, H.-P. Hollenbach, J. Shen, M. Oberle, D. Szczerba, A. Kam, J. W. Guag, and N. Kuster, "The Virtual Family - development of surface-based anatomical models of two adults and two children for dosimetric simulations," *Phys. Med. Biol*., vol. 55, pp. N23-N38, Jan. 2010.

[4] M. C. Gosselin, E. Neufeld, H. Moser, E. Huber, S. Farcito, L. Gerber, M. Jedensjö, I. Hilber, F. Di Gennaro, B. Lloyd, E. Cherubini, D. Szczerba, W. Kainz, and N. Kuster, "Development of a New Generation of High-Resolution Anatomical Models for Medical Device Evaluation: The Virtual Population 3.0," *Phys. Med. Biol*., vol. 59, no. 18, pp. 5287-5303, online August 21, 2014.

[5] X. G. Xu and K. F. Eckerman, *Handbook of Anatomical Models for Radiation Dosimetry*. Boca Raton: Taylor & Francis, 2010.

[6] U.S. National Library of Medicine. The Visible Human Project® Online: http://www.nlm.nih.gov/research/visible/visible_human.html

[7] M. Iacono, E. Neufeld, E. Akinnagbe, K. Bower, J. Wolf, I. Oikonomidis, D. Sharma, B. Lloyd, B. Wilm, M. Wyss, K. Pruessmann, A. Jakab, N. Makris, E. Cohen, N. Kuster, W. Kainz, and L. Angelone, "MIDA: A Multimodal Imaging-Based Detailed Anatomical Model of the Human Head and Neck," *PLoS ONE*, vol. 10, no 4, online April 22, 2015.

[8] M. Bikson, A. Rahman, and A. Datta, "Computational models of transcranial direct current stimulation," *Clinical EEG and Neuroscience*, vol. 43, pp. 176-183, July 2012.

[9] P.C. Miranda, A. Mekonnen, R. Salvador, and G. Ruffini, "The electric field in the cortex during transcranial current stimulation," *NeuroImage*, vol. 70, pp. 48-58, April 2013.

[10] M. Bikson, A. Rahman, A. Datta, F. Fregni, and L. Merabet, "High-resolution modeling assisted design of customized and individualized transcranial direct current stimulation protocols," *Neuromodulation: Technology at the Neural Interface*, vol. 15, pp. 306-315, July 2012.

[11] M. Bikson and A. Datta, "Guidelines for precise and accurate computational models of tDCS," *Brain Stimulation*, vol. 5, pp. 430-434, July 2012.

[12] J. M. Elloian, G.M. Noetscher, S.N. Makarov, and A. Pascual-Leone, "Continuous wave simulations on the propagation of electromagnetic fields through the human head," *IEEE Trans. Biomedical Engineering*, vol. 61, no. 6, pp. 1676-1683, June 2014.

[13] G.M. Noetscher, J. Yanamadala, S.N. Makarov, and A. Pascual-Leone, "Comparison of cephalic and extracephalic montages for Transcranial Direct Current Stimulation - A numerical study," *IEEE Trans. Biomedical Engineering*, vol. 61, no. 9, pp. 2488-2498, Sep. 2014.

[14] A. M. Helderman, N. S. Thang, T. Dolma, T. T. Trinh, M. W. Piazza, J. Zhang, J. Yanamadala, and S. N. Makarov, "Using MATLAB® platform for image segmentation and FEM-compatible triangular surface mesh generation – vertebral column of Visible Human Project – Female," EMBC 2015, Undergraduate Poster, under review.

[15] M. Kozlov, G. M. Noetscher, A. Nazarian, and S. N. Makarov, "Comparative analysis of different hip implants within a realistic human model located inside a 1.5T MRI whole body RF Coil," EMBC 2015, accepted.

[16] W. P. Segars, G. Sturgeon, S. Mendonca, J. Grimes, and B. M. Tsui, "4D XCAT phantom for multimodality imaging research," *Med. Phys.*, vol. 37, no 9, pp. 4902-4915, Sep. 2010.

[17] J. Lee, D. K. Sun and Z. J. Cendes, "Full-Wave Analysis of Dielectric Waveguides using Tangential Vector Finite Elements", *IEEE Transactions on Microwave Theory and Techniques*, vol. 39, no. 8, pp. 1262-1271, Aug. 1991.